Chemical Engineering Science 267 (2023) 118376

Contents lists available at ScienceDirect

Chemical Engineering Science

journal homepage: www.elsevier.com/locate/ces

Non-thermal plasma assisted CO_2 conversion to CO: Influence of non-catalytic glass packing materials

M. Umamaheswara Rao [a], K.V.S.S. Bhargavi [a], Piu Chawdhury [a], Debjyoti Ray [a], Siva Rama Krishna Vanjari [b], Ch. Subrahmanyam [a,*]

[a] Department of Chemistry, Indian Institute of Technology Hyderabad, Kandi, Sangareddy, Telangana 502285, India
[b] Department of Electrical Engineering, Indian Institute of Technology Hyderabad, Kandi, Sangareddy, Telangana 502285, India

HIGHLIGHTS

- Carbon dioxide conversion was achieved by an NTP-DBD model.
- The effect of non-catalytic material packing on CO_2 conversion was investigated.
- The packed DBD reactor has shown a higher efficiency than the unpacked DBD reactor.
- Plasma discharge characteristics were affected by the packing materials.

ARTICLE INFO

Article history:
Received 11 August 2022
Received in revised form 28 November 2022
Accepted 2 December 2022
Available online 9 December 2022

Keywords:
CO_2 conversion
DBD plasma
Energy efficiency
Non-catalytic materials

ABSTRACT

The current research is focused on the decomposition of carbon dioxide (CO_2) into carbon monoxide (CO) and oxygen (O_2) in a non-thermal plasma reactor using dielectric barrier discharge (DBD) at ambient conditions. Pure CO_2 was injected into the DBD reactor at a flow rate of 30 mL min^{-1}, and the voltage was varied between 16 kV to 22 kV. The filamentary micro discharges generated during plasma has a significant effect on CO_2 conversion. The effect of packing materials on CO_2 conversion was investigated by packing non-catalytic materials such as quartz wool, glass capillary, glass wool, and glass beads in the discharge zone of the DBD reactor. Among the studied packing materials, quartz wool exhibited a maximum CO_2 conversion of 9.3 % at a discharge power of 2.0 W and specific energy input (SEI) of 4.0 J mL^{-1}. However, glass capillary exhibited the highest energy efficiency of 1.2 mmol kJ^{-1} at an SEI of 3.5 J mL^{-1}.

1. Introduction

The rising demand for energy in modern society has resulted in the substantial use of traditional carbon-containing fossil fuels, releasing significant amounts of greenhouse gases (CO_2, CH_4, and NO_2) into the environment (Lashof and Ahuja, 1990). CO_2 concentrations have increased from 280 ppm in the preindustrial era to 410 ppm in current times (Retallack and Conde, 2020). Atmospheric carbon dioxide concentrations have continuously increased, negatively impacting the environment by exponentiating the greenhouse effect and global warming (Friedlingstein et al., 2010). Therefore, it is the need of the hour to find proper ways to decrease CO_2 levels in the atmosphere. Several techniques are available such as carbon capture and utilization (CCU), and carbon capture and storage (CCS) have shown promise in lowering CO_2 emissions (Gibbins and Chalmers, 2008). CCS is not a long-term solution for reducing greenhouse gas emissions. It entails high cost, little acceptance from the public, and the possibility of leakage during or after injection. As a result, developing new sustainable options with minimal or no environmental effect and zero CO_2 emissions are essential (Cuéllar-Franca and Azapagic, 2015).

Carbon capture and utilization (CCU) is a potential strategy for reducing carbon emissions in the long term (Ghiat and Al-Ansari, 2021). The CO_2 generated during industrial operations can be extracted, separated, and used as a feedstock to synthesize value-added products (Mei and Tu, 2017). The captured CO_2 can be converted into high-value-added chemicals and fuels (e.g., methanol, CH_4, CO, and DME) (Lu et al., 2018). However, as CO_2 is a stable and inert molecule, converting CO_2 in a cost-effective manner is a significant problem (George et al., 2021). Thermodynamical calculations suggest that to achieve higher CO_2 conversion, nearly 3500 K is needed, implying that the thermal decomposition of CO_2 will be highly energy-intensive (Parastaev et al., 2018).

* Corresponding author.
E-mail address: csubbu@iith.ac.in (Ch. Subrahmanyam).

https://doi.org/10.1016/j.ces.2022.118376
0009-2509/

$$CO_2 \rightarrow CO + \tfrac{1}{2} O_2 \quad \Delta H = 283 \text{ kJ mol}^{-1}$$

Carbon monoxide (CO) is one of the most significant chemical feedstocks. CO is a widely utilized industrial gas in the manufacture of bulk chemicals. For example, aldehydes can be produced from the hydroformylation of alkene with carbon monoxide and hydrogen (Cai et al., 2021). Methanol also can be synthesized by hydrogenating carbon monoxide (Farahani et al., 2022; Wang et al., 2018). Various approaches for converting CO_2 into valuable chemicals and fuels have been proposed in recent years, including thermal conversion (Galadima and Muraza, 2019), photochemical conversion (Zeng et al., 2018), electrochemical conversion (Qiao et al., 2014), and biological methods (Skjånes et al., 2007). In this context, non-thermal plasma (NTP) technology has received much attention on CO_2 conversion as it can work in any environment (Xu et al., 2017). However, a few catalysts have been studied to convert CO_2 to CO in plasma reactors. Danhua et al. (2015) studied the CO_2 conversion in a DBD plasma reactor packed with $BaTiO_3$, reported a 28 % CO_2 conversion at 50 W power and obtained an energy efficiency of 0.255 mmol/kJ (Mei et al., 2014). Zhang et al. (2017) studied CO_2 conversion with a Ni/SiO_2 catalyst in a DBD reactor filled with either $BaTiO_3$ or glass beads (Zhang et al., 2017). Yiming et al. (2015) studied with the photocatalyst $ZnO/g\text{-}C_3N_4$ for high-efficiency CO_2 conversion (He et al., 2015).

In an NTP reactor, the existence of energetic electrons can start the reaction under moderate circumstances. Various NTP designs have been tested, including glow discharge, microwave discharge, corona discharge, gliding arc discharge, radio frequency discharge, and dielectric barrier discharge reactor (DBD). DBD was recently used to evaluate CO_2 conversion, surface treatment, sewage degradation, and VOC removal (Nguyen et al., 2018). As compared to other NTPs such as radiofrequency, microwave plasma (Huang et al., 2017), corona discharge plasma (Babaeva and Naidis, 2021), and gliding arc plasma (Indarto et al., 2007), DBD offers two benefits. Firstly, The plasma equipment from DBD is simple to scale up because of its basic construction, making it an excellent approach for industrial scale (Damideh et al., 2020). Secondly, DBD can be easily integrated with packing material, which improves numerous reactions, and it produces high-energy electrons, with average electron energy of 1–10 eV, creating uniform discharge (Ray et al., 2016). The primary purpose of the dielectric barrier material is to limit electric current, thereby preventing the formation of sparks. By limiting the number of discharges and distributing micro discharges over the entire surface area of the dielectric barrier, the physical properties of the dielectric barrier can also influence the DBD characteristics (Alliati et al., 2018). As a result, dissociation, electron impact ionization, and excitation happen at room temperature leading to the generation of reactive species such as radicals, ions, excited atoms, or molecules (Kozák and Bogaerts, 2014). Hence, NTP can be employed as a substitute for traditional high-temperature catalytic chemical processes.

The packing material used in a DBD reactor plays a key role in CO_2 decomposition. It enhances the local electric field strength at a contact point between the material and improves CO_2 conversion and energy efficiency (Michielsen et al., 2017). This study explores the direct breakdown of pure CO_2 into CO and O_2 in a cylindrical DBD reactor containing non-catalytic material at low temperatures. To understand the effect of packing materials on plasma interactions during the CO_2 conversion, on the performance of the reactor, and on the physical aspects of the discharge, different packing materials such as glass capillary, glass wool, glass beads, and quartz wool were studied.

2. Experimental

2.1. Experimental setup

A coaxial dielectric barrier discharge (DBD) was constructed in this work for the plasma non-catalytic conversion of pure CO_2 into CO and O_2 at a low temperature. The schematic representation of the experimental setup is shown in Fig. 1. The plasma discharge was generated inside a cylindrical quartz tube. The quartz tube has an outer diameter of 23 mm and an inner diameter of 20 mm. Stainless steel (SS) rod (11 mm dia) is provided along the length of the quartz tube axis and connected to a high voltage power source. A ground electrode was created by wrapping a stainless-steel mesh around the circumference of the quartz tube,

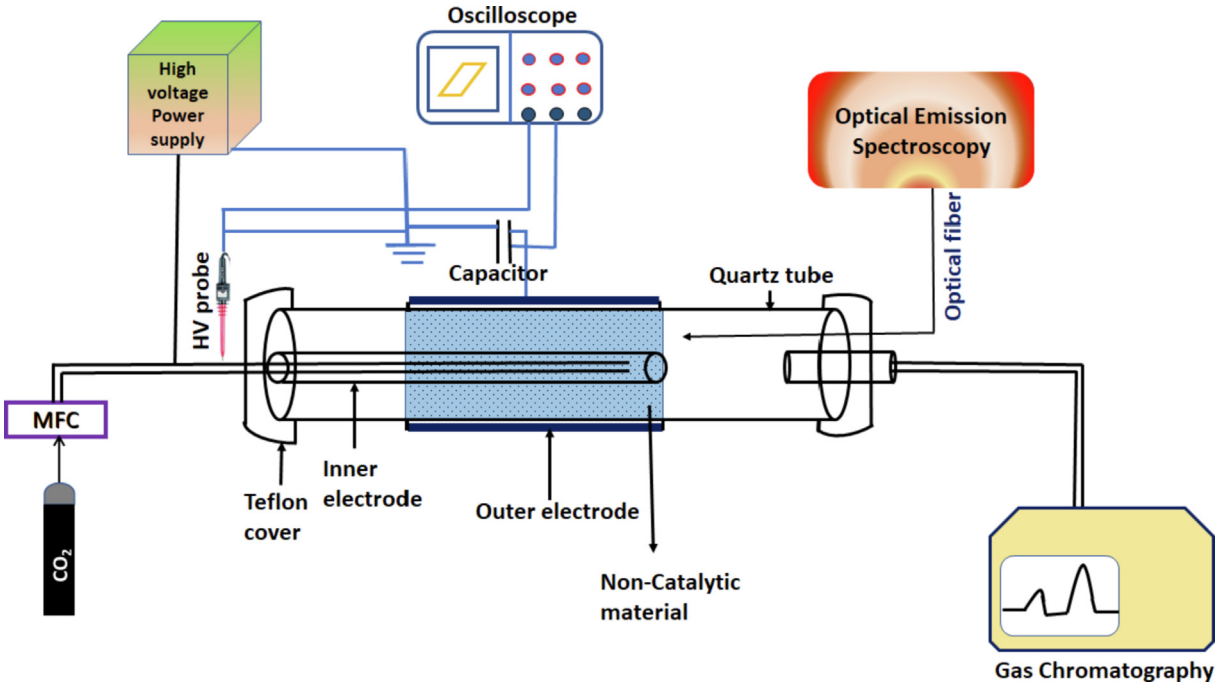

Fig. 1. Schematic representation of the DBD reactor.

and it was grounded through a capacitor (4 μF). The reactor has a discharge gap of 4.5 mm, and a discharge volume of 24 cm^3. The plasma discharge was created by changing an alternating high voltage from 16 kV to 22 kV with 50 Hz. A high voltage probe, Agilent 34136A, was used to measure the applied voltage, and a digital oscilloscope (Tektronix TDS2014B) was used to record the discharge electrical signals.

The Q–U Lissajous figure was used to calculate the discharge power (Wang et al., 2021). The CO_2 inlet gas flow rate was controlled by a mass flow controller (MFC17, Aalborg, USA), and the flow rate was fixed at 30 mL min^{-1}. The outlet from MFC was directly connected to the inner electrode of the DBD reactor, where the DBD plasma discharge was generated between two electrodes by varying the applied voltage. For the present study, we have used glass beads (25 g), glass wool (18 g), glass capillary (17 g), and quartz wool (1.2 g). The packing was done in such a way as to completely fill the discharge volume (24 cm^3) and discharge zone (11 cm). The dielectric constant of glass materials ~ 4 and quartz wool ~ 5.

2.2. Gas analysis and parameter definitions

The feed gas composition and the products formed were analyzed using a gas chromatography instrument (GC2014 SHIMADZU) with a packed column (Porapak-Q, 3 m, 80/100 mesh) and a thermal conductivity detector (TCD).

The CO_2 conversion, CO selectivity, and CO yield are defined as follows:

$$CO_2\ \text{Conversion}\ (\%) = \frac{\text{Converted } CO_2\ \left(\text{mmol min}^{-1}\right)}{CO_2\ \text{input}\ \left(\text{mmol min}^{-1}\right)} \times 100 \tag{1}$$

$$\text{CO Selectivity}\ (\%) = \frac{\text{CO formed}\ (\text{mmol min}^{-1})}{CO_2\ \text{converted}\ (\text{mmol min}^{-1})} \times 100 \tag{2}$$

$$\text{CO yield}\ (\%) = \frac{\text{CO formed}\ (\text{mmol min}^{-1})}{CO_2\ \text{input}\ (\text{mmol min}^{-1})} \times 100 \tag{3}$$

Energy efficiency is defined as the ratio of converted CO_2 to discharge power

$$\text{Energy efficiency}\ (\text{mmol kJ}^{-1}) = \frac{\text{Converted } CO_2\ \left(\text{mmol min}^{-1}\right)}{\text{Power (W)}} \times \frac{1000}{60} \tag{4}$$

Specific energy input stands for the energy consumption per mL of gas volume, and it is calculated by using the following equation

$$\text{Specific energy input}\ (\text{J mL}^{-1}) = \frac{\text{Discharge Power (W)}}{\text{Total gas flow rate}\ (\text{mL min}^{-1})} \times 60 \tag{5}$$

The carbon balance (C_B) is calculated as follows

$$\text{Carbon balance}\ (\%) = \frac{CO_2\ \text{Output}\ \left(\text{mmol min}^{-1}\right) + \text{CO formed}\ (\text{mmol min}^{-1})}{CO_2\ \text{input}\ (\text{mmol min}^{-1})} \times 100 \tag{6}$$

3. Results and discussion

3.1. Effect of packing materials on discharge power and discharge characteristics

The discharge characteristics will be modified when a dielectric material is introduced into the DBD plasma. Fig. 2 clearly distinguishes between plasma-only discharge and that of the non-catalytic packed DBD discharges. The electric field shows filamentary discharges when no packing material was inside the discharge zone. The local electric field generates more intense filaments on the surface of the inner electrode (Fig. 2a). We can observe that when non-catalytic material is added to the discharge gap, the nature of the discharge totally changes. In essence, it creates the packed bed discharge effect (Chen et al., 2008). Glass beads minimize the discharge volume in the discharge gap and prevent the production of filamentary streamers, which leads to the formation of the more common surface discharges (Fig. 2b). In contrast, the enhanced filaments produced exclusively by the sharp edges of the capillary tubes cover the whole discharge volume (Fig. 2c). Fig. 2d shows that glass wool has more intense sparks than glass beads and capillaries because of the micro-corona discharges produced between the porous fibers. Fig. 2e shows an increase in micro discharge filaments across the quartz wool. Compared to the typical discharges formed among all the packed materials, quartz wool with DBD exhibits brighter intensity.

The power dissipated during the plasma discharge was estimated according to the Q-U Lissajous figure, as shown in Fig. 3a. The area of the Lissajous figure increases when the discharge zone is packed with non-catalytic materials, compared to a DBD alone system. Among the various packing materials, quartz wool packaging displays the highest power of 2.0 W at an applied voltage of 22 kV. This might be due to the quartz wool in the discharge zone facilitating the increase in the magnitude of multiple current spikes in the plasma (Gallon et al., 2012). Fig. 3b shows the effect of various packing materials on average power dissipation as a function of applied voltage. The quartz wool displayed the highest power at all applied voltages. It can be observed that the discharge power followed the trend quartz wool > glass wool > glass capillary > glass beads > no packing.

The effect of specific energy input has been shown in Fig. 4a. DBD with quartz wool at 22 kV produced the highest specific energy input at 4.0 J mL^{-1} compared to an SEI of 2.4 J mL^{-1} DBD alone. Fig. 4a shows that the energy input into the plasma discharge zone improved when the discharge power was increased. Fig. 4b shows the total charge transferred per half-cycle as a function of applied voltage. Various plasma parameters calculated from the Lissajous figures are listed in Table 1. Under non-catalyst packing conditions, the discharge power, charge transfer per half cycle, and effective capacitance are higher than DBD alone. High-energy, active plasma particles are directly responsible for reactions with increasing specific energy input.

3.2. Effect of packing materials on discharge characteristics

Table 1 shows that the discharge characteristics change noticeably for the plasma reactor with and without packing. Even though there was no significant change in the discharge parameters when different non-catalytic materials were used, the average electric field was increased when non-catalytic materials were used instead of the DBD alone. As a result, it can be inferred that the packing material can influence on the reaction performance.

When non-catalytic materials were placed in the DBD reactor, the reduced electric field was enhanced by following the order

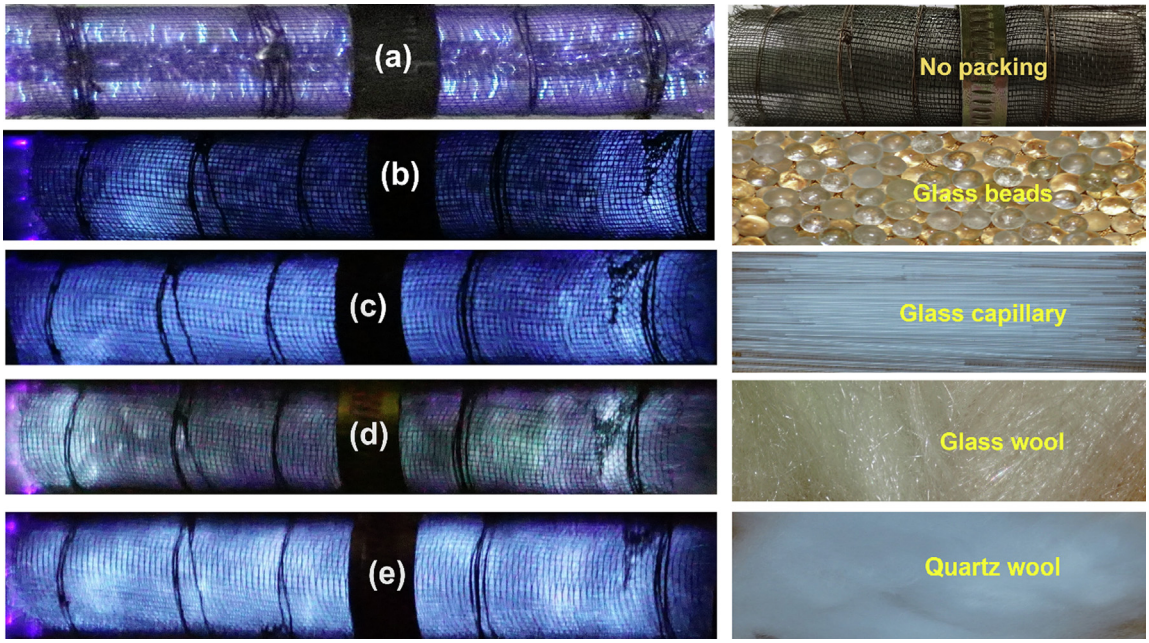

Fig. 2. Images of the CO_2 DBD plasma (a) no packing, (b) Packed with glass beads (c), Packed with glass capillary, (d) Packed with glass wool, and (e) Packed with quartz wool (discharge length: 11 cm, discharge gap: 4.5 mm, applied voltage: 22 kV, Frequency 50 Hz, Flow rate 30 mL min^{-1} inner electrode: Stainless steel rod, Outer electrode: stainless steel mesh).

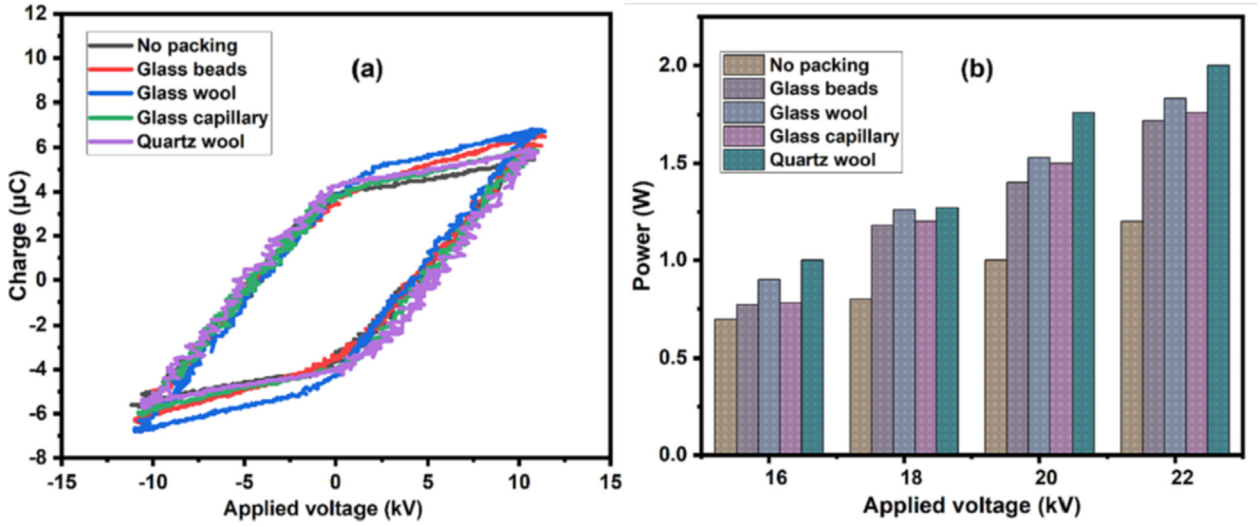

Fig. 3. (a) The Lissajous figure for different packed materials in the discharge zone at 22 kV (b) Power dissipated as a function of applied voltage for different packing conditions (gas flow rate: 30 mL min^{-1}; applied frequency: 50 Hz).

shown in Fig. 5a: Plasma + Quartz wool > Plasma + Glass capillary > Plasma + Glass beads > Plasma + Glass wool > Plasma alone. Because of this, charge deposition on the surface of these non-catalytic materials is permitted. As dielectric materials efficiently collect charges on their surface, charge transmission between electrodes is improved. Because of this, the average electric field is slightly increased from 10 kV cm^{-1} (Plasma alone) to 11.50 kV cm^{-1} (Quartz wool + Plasma).

In addition, the intensity of the local electric field at the point of contact between the materials has been enhanced. The electron energy distribution function and the mean electron energy were determined using the Boltzmann equation solver software BOLSIG+ (Version −11/2019) (Carbone et al., 2021; Pitchford et al., 2017; Pancheshnyi et al., 2012; Hagelaar and Pitchford, 2005). Plasma alone, Plasma + Glass wool, Plasma + Glass beads, Plasma + Glass capillary, and Plasma + Quartz wool were the sequences in which the discharge's mean electron energy was measured. The change of the mean electron energy as a function of the reduced electric field is shown in Fig. 5b for both plasma and plasma with packed materials. A DBD plasma with packing materials produces more electrons having high energy. From Fig. 5b, the mean electron energy of the system is 1.79 eV. This is in good agreement with the reduced electric field order.

3.3. Packed bed DBD for CO_2 decomposition

The applied voltage varied between 16 kV and 22 kV at a fixed flow rate of 30 mL min^{-1} CO_2 to investigate the influence of SEI on reactant conversion and product yield. DBD plasma gets ignited when the electric field strength is high enough to cause the electri-

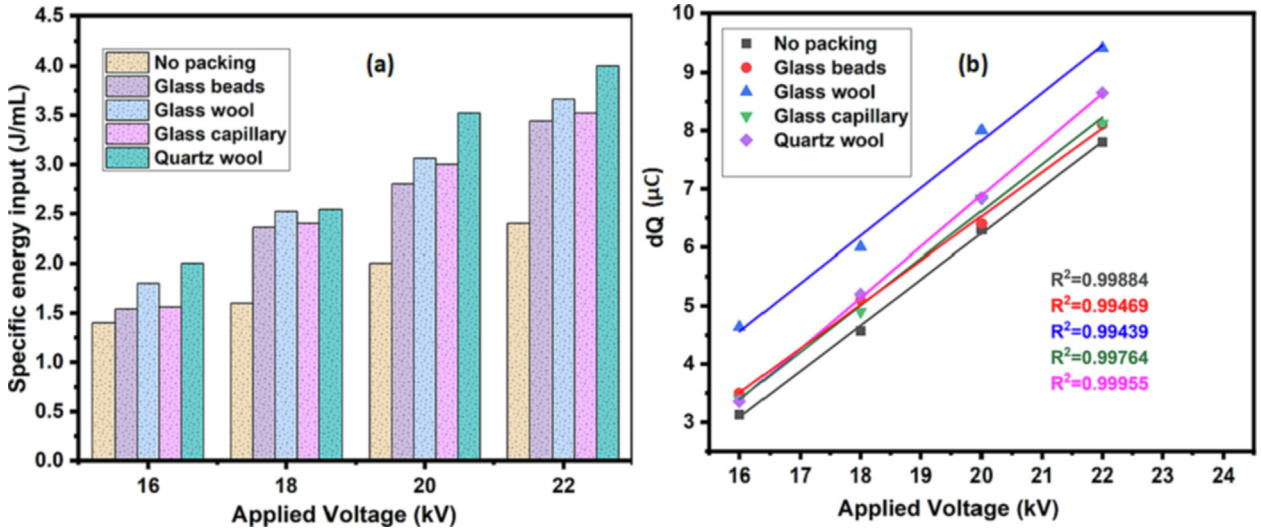

Fig. 4. (a) Specific energy input with applied voltage varied from 16 kV to 22 kV (b) The total charge transferred per half-cycle as a function of applied voltage (gas flow rate: 30 mL min^{-1} and frequency: 50 Hz).

Table 1
Comparison of plasma parameters for different packing conditions.

Packing material	Applied Voltage (kV)	Power (W)	C_d (μF)	Q pk-pk (μC)	dQ (μC)	U_b (kV)	E (kV cm^{-1})	E/N (Td)
No packing	22	1.2	0.85	10.5	7.8	4.5	10.0	37.2
Glass beads	22	1.72	0.92	12.5	8.1	3.4	10.84	40.3
Glass wool	22	1.83	1.0	13.5	9.4	4.0	10.45	39.0
Glass capillary	22	1.76	0.91	11.9	8.12	4.1	11.2	41.7
Quartz wool	22	2.0	0.97	12.0	8.65	4.4	11.5	42.8

C_d = Dielectric capacitance, $Q_{pk\text{-}pk}$ = Peak to peak charge, dQ = Charge transfer per half cycle, U_b = Breakdown voltage, E = Average electric field, E/N (Td) = Reduced electric field.

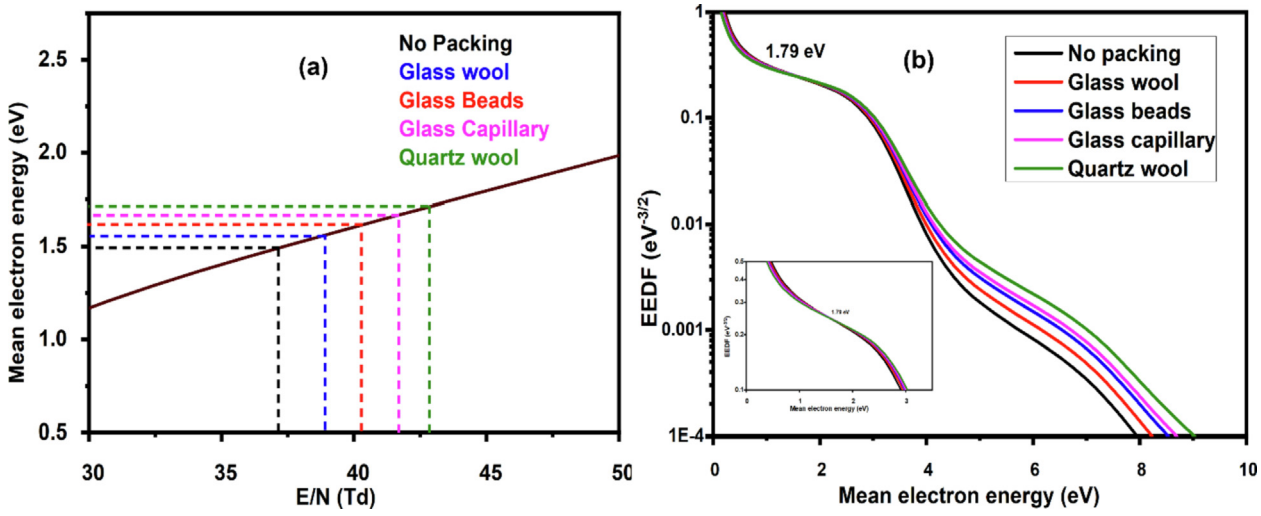

Fig. 5. (a) Calculated mean electron energy vs reduced electric field (b) Electron energy distribution function vs mean electron energy.

cal breakdown, resulting in many filamentary micro discharges that provide conductive channels for electrons to flow throughout the discharge gap (Chawdhury et al., 2019). The electrons interact with CO_2 molecules during plasma discharge and dissociate them via electron impact dissociation, which is considered one of the dominant reactions when converting CO_2 in a DBD reactor. In plasma processing of CO_2, it is also possible to have electron dissociation and electron impact ionization (Yap et al., 2015). The CO_2 conversion begins with the following plasma reactions:

$$e^- + CO_2 \rightarrow CO(g) + O(g) + e^-(R1)$$

$$e^- + CO_2(g) \rightarrow CO(g) + O^-(g)(R2)$$

$$e^- + CO_2(g) \rightarrow CO_2^+(g) + 2e^-(R3)$$

Previous experimental and simulation studies indicated that by increasing the discharge power at a constant frequency, the discharge's electric field, electron density, and gas temperature

improve (Petrović et al., 2009; Li et al., 2008), thus enhancing the conversion of reactant gas. Packing the discharge zone with high dielectric constant materials generates a homogeneous discharge and enhanced field strength. Fig. 6 shows that maximum CO_2 conversion of ~ 9.3 % was achieved with quartz wool packed DBD at 22 kV. As a function of the reduced electric field (E/N), the fraction of the energy that is transferred to the different channels of CO_2 excitation, ionization, and dissociation. If the average temperature of the electrons in the NTP is 1–2 eV or if the reduced electric field (E/N) is 20–40 Td, about 97 % of the total plasma energy can be transferred to CO_2 that is excited by vibrational- vibrational relaxation (George et al., 2021). The enhancement of the average electric field by the packing material increases the production of reactive species and the density of electrons in the plasma, allowing for a greater amount of CO_2 to be converted without a corresponding increase in discharge power, Therefore, it may be possible to improve energy efficiency by using appropriate packing materials in the discharge zone.

Glass capillary, glass wool, and glass beads have the same dielectric constant, which is lesser than quartz. Quartz wool (made up of fragile and flexible fibers of quartz) had a cotton wool appearance, which showed more discharges in the discharge zone. Also, these glass materials affect the CO_2 conversion. Glass capillary, which has a hollow cylindrical shape, shows more charge accumulation on the surface during the discharge than glass wool (spongy honeycomb) and glass beads (spherical). The magnitude of the discharge created in the plasma zone during voltage applications follows the trend: Quartz wool > Glass capillary > Glass wool > Glass beads > No packing. The voids between dielectric materials exhibit a strong electric field due to micro discharges and strong electric field variations. Also, dielectric materials boost discharge strength, leading to increased CO_2 conversion. Quartz wool has a higher dielectric constant among all non-catalytic materials used in the study (Michielsen et al., 2017). The non-porous and non-adsorbing properties of the glass materials and their dielectric nature (the ability to accumulate charge on the surface) eliminate the possibilities of catalytic effects. The amplitude of multiple current spikes in the plasma is increased when quartz wool is present in the discharge zone. It indicates that the current pulses' strength has been increased. Hence, quartz wool has the highest power. The possibility of CO_2 conversion in the reactor is affected by the increase in high-energy particles, resulting in more C=O bond breakage leading to higher CO_2 decomposition into CO and O_2.

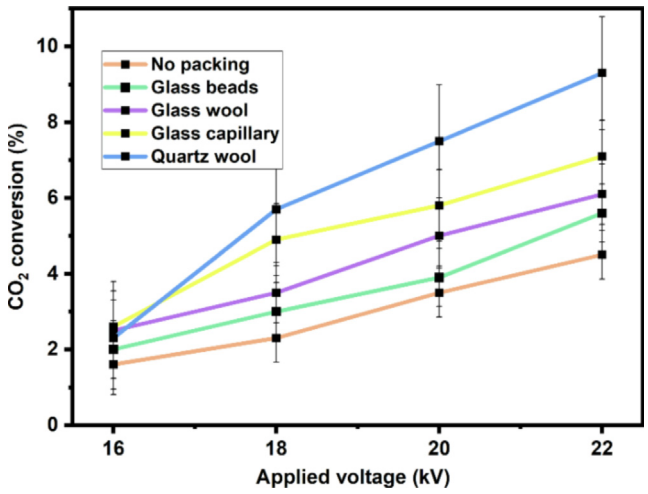

Fig. 6. Conversion of CO_2 with applied voltage with various packing materials (Applied frequency 50 Hz).

3.4. Effect of packing material on the selectivity and yield of the product

Fig. 7a represents varied packing circumstances that show the effect of applied voltage on the selectivity of the predicted product, CO. The CO selectivity decreased with increased applied voltage and increased CO_2 conversion for all reactions investigated in this study. This might be due to the Boudouard reaction or carbon production due to direct breakdown (Gallon et al., 2012). With no packing, we achieved approximately 100 % CO selectivity at 16 kV, but with packing materials, CO selectivity was decreased when the applied voltage was raised. This is due to the formation of solid carbon in the reaction, which was adsorbed on the surface of the inner electrode and walls of the quartz tube. CO selectivity of 65 % was achieved using quartz wool packing at 22 kV. The CO selectivity might have failed to reach 100 % due to the following reactions. At the highest discharge power, CO can be converted to CO_2 and solid carbon (C).

$$2CO \rightarrow CO_2 + C(i)$$

$$CO_2 \rightarrow C + O_2(ii)$$

Reaction (ii) is more complex than reaction (i); moreover, non-catalytic materials do not have enough surface area for carbon deposition. Fig. 7b indicates the CO yield (%) during the CO_2 decomposition reaction at different applied voltages. CO yield increased as applied voltage, power and SEI increased regardless of packing. This might be because the presence of highly energetic electrons generated at high applied power density has contributed to the maximum CO_2 decomposition. The maximum yield of CO obtained when quartz wool was combined with DBD at 2.0 W power was 6.1 %, whereas DBD alone yielded 3.1 % at the discharge power of 1.2 W.

3.5. Energy efficiency and carbon balance

The number of moles of gas converted per unit of plasma power was used to calculate a plasma reactor's energy efficiency for gas conversion (Equation (4)). The energy efficiency is shown in Fig. 8a. The maximum energy efficiency calculated was 1.2 mmol kJ^{-1} for DBD with glass capillary. The lowest energy efficiency was 0.83 mmol kJ^{-1} for DBD alone.

Fig. 8b depicts carbon balance related to the unconverted CO_2 and carbon-containing gaseous products generated during the reaction as defined in Equation (6). Carbon balance was nearly 100 % at the lowest applied voltage of 16 kV with packed DBD and DBD alone. There was a decrease in carbon balance with the increase in applied voltage. This might be because of the unreacted solid carbon deposition on the reactor walls and the surfaces of the internal electrodes. Carbon balance at 22 kV was 96.5 %, with quartz wool packing at the maximum discharge power of 2.0 W.

Table 2 shows the comparison of CO_2 conversion, CO selectivity, and the energy efficiency of the present study with the reported literature. From the table, it can be inferred that a reasonable CO_2 conversion can be obtained with a DBD reactor packed with non-catalytic materials compared to a DBD reactor with catalytic materials.

3.6. The impact of closely packed materials on reaction rates

Fully packed materials in the discharge zone are used to improve CO_2 decomposition. The following equation was used to determine the decomposition rate constant according to the first-order kinetic model.

$$\ln\left(C_{in}/C_{out}\right) = (SEI) \times K + C$$

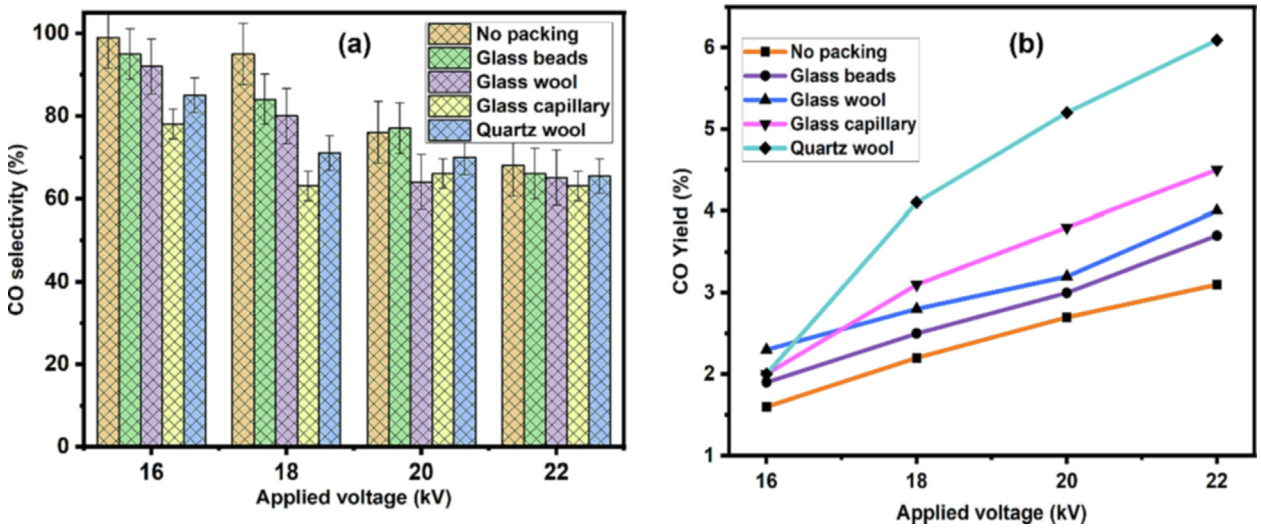

Fig. 7. (a) Effect of applied voltage on the CO selectivity (b) Effect of packing materials on CO yield (%) at a constant gas flow rate of 30 mL min^{-1} and a fixed frequency of 50 Hz.

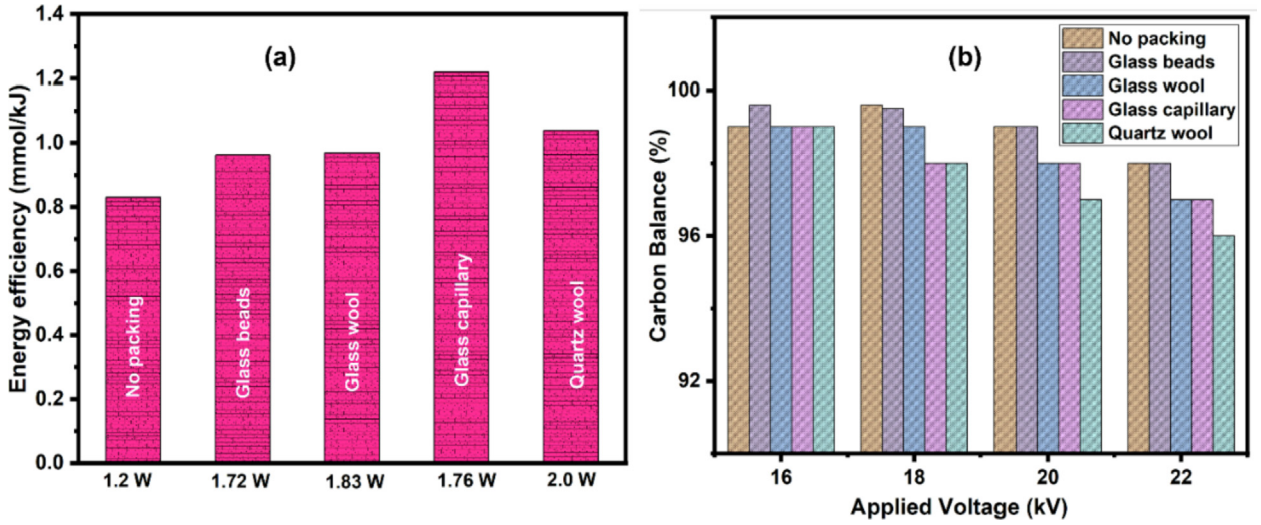

Fig. 8. (a) A comparison of Energy efficiency vs power at an applied voltage of 22 kV (b) Carbon balance as a function of applied voltage.

Table 2
A comparison study on CO_2 conversion.

Plasma	Power (W)	Flowrate (mL min^{-1})	Packed material	CO_2 conversion (%)	CO Selectivity (%)	Energy Efficiency (mmol/kJ)	References
DBD	2.4	30	5 %ZnO + g-C_3N_4	12	70	1.1	(Ray et al., 2020)
DBD	2.2	30	15 % CuO/Al_2O_3	15.7	48	1.597	(Ray et al., 2021)
DBD	28	60	$BaTiO_3$	38	–	0.6	(Mei et al., 2016)
DBD	55	150	Molecular Sieves 5A	25	63	–	(Wang et al., 2017)
DBD	50	50	Glass beads	~21	~ 95	~0.17	(Mei et al., 2014)
DBD	15.8	41.9	No packing	14.3	–	0.285	(Mei et al., 2016)
DBD	100	50	Glass wool	10	–	–	(Michielsen et al., 2017)
DBD	2.0	30	Quartz wool	9.3	65	1.039	This work

SEI is the specific energy input, K is the decomposition rate constant, C is the intercept, and C_{in} and C_{out} represent CO_2 input and output concentrations, respectively. Fig. 9 shows the linear relationship between the ln (C_{in}/C_{out}) as a function of SEI for various packing materials. The corresponding decomposition rate constants were 0.0244, 0.020, 0.017, 0.016, and 0.019 for quartz wool, glass capillary, glass wool, glass beads, and no packing, respectively. The maximum decomposition rate obtained for Quartz

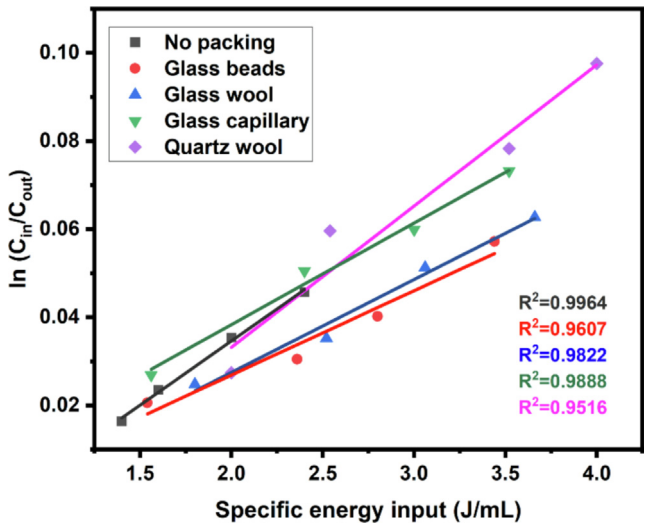

Fig. 9. The plot of ln (C_{in}/C_{out}) vs SIE for different packing materials.

wool-DBD indicates that it has the best CO_2 decomposition capacity.

3.7. Reaction stability and gas phase reaction

The DBD plasma CO_2 conversion reaction over quartz wool was run at a constant flow of 30 mL min^{-1} at 20 kV for 420 min at low temperature and atmospheric pressure to study the stability of the reaction. Fig. 10a shows the conversion of CO_2 and selectivity of CO. It has been observed that the CO_2 conversion and CO selectivity are stable after 420 min of the reaction.

Fig. 10b represents the schematic diagram of the gas phase reaction mechanism. Although the CO is very stable, it can recombine with an oxygen atom and form CO_2 at long enough residence time. This might be one of the reasons for less conversion of CO_2. Interestingly, compared to no packed condition, more conversion of CO_2 was observed by non-catalytic packed material, indicating that the surface discharge of packed materials plays an important role in CO_2 DBD plasma. There is a possibility of quick recombination of oxygen atoms among themselves and forms O_3 and O_2 (Bogaerts et al., 2015).

3.8. Optical emission spectroscopy

Optical emission spectroscopy (OES) is an excellent tool for better understanding of the properties of active species produced in plasma. The optical emission spectroscopy was recorded using a Princeton Instrument Action SpectraPro® SP-2300 equipped with 600 g mm^{-1} gratings with 500 nm Blaze. The spectra is recorded with only plasma and with quartz wool packed DBD plasma separately to understand the excited species created. We have recorded the OES while avoiding the air discharge between the dielectric and the outer electrode by keeping the optical fiber inside the quartz tube, as shown in the Fig. S3. As a result, the observed peaks were essentially identical under all circumstances. Fig. 11 displays the peak assignment for the active species, which include CO_2, CO, CO_2^+, and CH. The CO_2 dissociation might be due to vibrational relaxation as CO_2 splitting in DBD plasma is probably caused by vibrational excitation (Devia et al., 2015; Hou et al., 2016). The peak at 314.4 nm ($C^2\sum$ - $X^2\prod$) represents CH emission due to the traces of moisture present in the CO_2 gas cylinder. The CO_2^+ ion is responsible for most of the prominent peaks in the CO_2 spectrum from The Fox-Duffendack Barker transition system (Pearse et al., 1976). The wavelength bands corresponding to CO_2^+ are at 339.3 nm, 358.8 nm and 370.3 nm (Garcia-Cosio et al., 2011; Wang et al., 2022). The peak at 391 nm is caused by CO_2 $^1B_2$–$X^1\Sigma^+$ transition (Ray et al., 2020; Ray et al., 2021). O_2 emission peaks around 406 nm (Quigley et al., 2016; Fan and Tahir, 2022; Zhu et al., 2014), and CO emission is responsible for the peaks seen around 450.5 nm, 484 nm, 517 nm and 558.4 nm (Garcia-Cosio et al., 2011; Wang et al., 2022; Khan et al., 2019).

4. Conclusions

The performance of CO_2 decomposition in a coaxial DBD reactor operating under ambient conditions has been explored in this work. The current research demonstrates that the DBD plasma reactor has the potential for converting CO_2 to CO. It was observed that the non-catalytic packing materials could significantly influence the CO_2 conversion. It was found that the performance of the DBD plasma reactor was improved by adding various packing materials to the discharge region. Typical CO_2 conversion results indicated Quartz wool > Glass capillary > Glass wool > Glass beads > DBD alone. The performance was most effective with quartz wool packing at 2.0 W and SEI of 4.0 J mL^{-1}, resulting in a

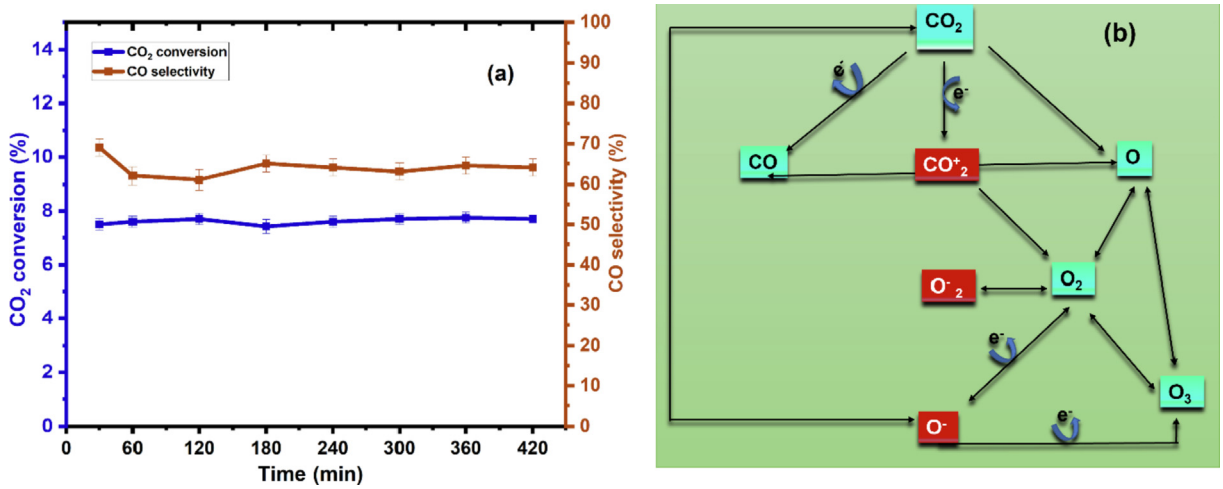

Fig. 10. (a) Shows the packed material stability as a function of time with quartz wool packed into the reactor (Total flow rate 30 mL min^{-1}, applied voltage 20 kV at fixed frequency 50 Hz) (b) shows the reaction pathways in the plasma CO_2 conversion.

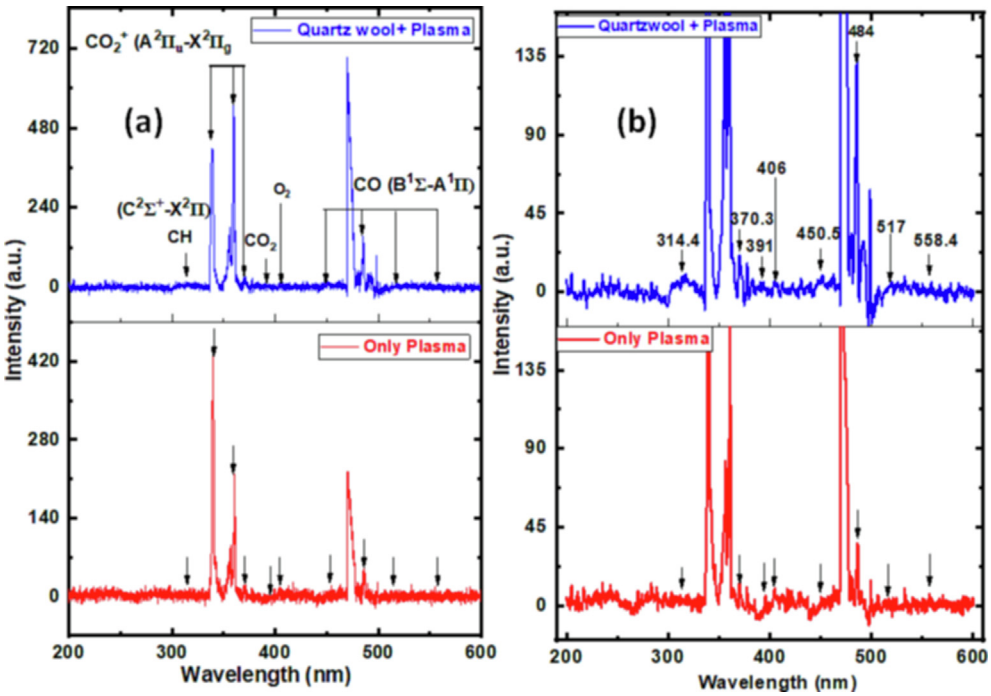

Fig. 11. CO_2 plasma emission spectrum. (Grating: 600 glue at 500 nm; applied voltage 18 kV and total flow rate 30 mL min^{-1}, (a) only plasma and plasma + quartz wool (b) Enlarged spectra of only plasma and plasma + quartz wool.

maximum CO_2 conversion of 9.3 %. With the glass capillary packed in the discharge zone, the maximum energy efficiency of 1.2 mmol kJ^{-1} was achieved.

CRediT authorship contribution statement

M. Umamaheswara Rao: Methodology, Conceptualization, Formal analysis, Software, Investigation, Writing - original draft. **K.V. S.S. Bhargavi:** Formal analysis, Software, Investigation. **Piu Chawdhury:** Visualization, Investigation. **Debjyoti Ray:** Visualization, Investigation, Software. **Siva Rama Krishna Vanjari:** Visualization. **Ch. Subrahmanyam:** Supervision, Project administration, Conceptualization, Writing - review & editing.

Data availability

Data will be made available on request.

Declaration of Competing Interest

The authors declare that they have no known competing financial interests or personal relationships that could have appeared to influence the work reported in this paper.

Acknowledgements

M. Umamaheswara Rao would like to thank the University Grants Commission, India for providing junior research fellowship. We acknowledge Indian Institute of Technology Hyderabad for the research facilities.

Appendix A. Supplementary material

Supplementary data to this article can be found online at https://doi.org/10.1016/j.ces.2022.118376.

References

Alliati, M., Mei, D., Tu, X., 2018. Plasma activation of CO2 in a dielectric barrier discharge: a chemical kinetic model from the microdischarge to the reactor scales. J. CO2 Util. 27, 308–319. https://doi.org/10.1016/j.jcou.2018.07.018.

Babaeva, N.Y., Naidis, G.V., 2021. On the efficiency of CO2 conversion in corona and dielectric-barrier discharges. Plasma Sources Sci. Technol. 30, 03LT03. https://doi.org/10.1088/1361-6595/abe6e6.

Bogaerts, A., Kozák, T., van Laer, K., Snoeckx, R., 2015. Plasma-based conversion of CO 2: current status and future challenges. Faraday Discuss. 183, 217–232. https://doi.org/10.1039/C5FD00053J.

Cai, J., Zheng, W., Luo, M., Kuang, C., 2021. Evaluation of the CO2 gasification of residual char under a regeneration atmosphere via calcium-based chemical looping gasification. Chem. Eng. Process. - Process Intensif. 168,. https://doi.org/10.1016/j.cep.2021.108564 108564.

Carbone, E., Graef, W., Hagelaar, G., Boer, D., Hopkins, M.M., Stephens, J.C., Yee, B.T., Pancheshnyi, S., van Dijk, J., Pitchford, L., 2021. Data needs for modeling low-temperature non-equilibrium plasmas: the LXCat project, history, perspectives and a tutorial. Atoms. 9, 16.

Pearse, R.W.B., Gaydon, A.G., Pearse, R.W.B., Gaydon, A.G., 1976. The identification of molecular spectra, 297. Chapman and Hall, London, p. 293.

Chawdhury, P., Ray, D., Nepak, D., Subrahmanyam, C., 2018. NTP-assisted partial oxidation of methane to methanol: effect of plasma parameters on glass-packed DBD. J. Phys. Appl. Phys. 52, 015204. doi: 10.1088/1361-6463/aae635.

Chen, H.L., Lee, H.M., Chen, S.H., Chang, M.B., 2008. Review of packed-bed plasma reactor for ozone generation and air pollution control. Ind. Eng. Chem. Res. 47, 2122–2130. https://doi.org/10.1021/ie071411s.

Cuéllar-Franca, R.M., Azapagic, A., 2015. Carbon capture, storage and utilisation technologies: a critical analysis and comparison of their life cycle environmental impacts. J. CO2 Util. 9, 82–102. https://doi.org/10.1016/j.jcou.2014.12.001.

Damideh, V., Chin, O.H., Gabbar, H.A., Ch'ng, S.J., Tan, C.Y., 2020. Study of ozone concentration from CO2 decomposition in a water cooled coaxial dielectric barrier discharge. Vacuum 177, 109370. doi: 10.1016/j.vacuum.2020.109370.

Devia, D.M., Rodriguez-Restrepo, L.V., Restrepo-Parra, E., 2015. Methods employed in optical emission spectroscopy analysis: a review. Ing. Cienc. 11, 239–267. doi: 10.17230/ingciencia.11.21.12.

Fan, W.K., Tahir, M., 2022. Recent developments in photothermal reactors with understanding on the role of light/heat for CO2 hydrogenation to fuels: a review. Chem. Eng. J. 427,. https://doi.org/10.1016/j.cej.2021.131617 131617.

Farahani, M.D., Zeng, Y., Zheng, Y., n.d. The application of nonthermal plasma in methanol synthesis via CO2 hydrogenation. Energy Sci. Eng. doi: 10.1002/ese3.1107.

Friedlingstein, P., Houghton, R., Marland, G., Hackler, J., Boden, T., Conway, T., Canadell, J., Raupach, M., Ciais, P., Le Quere, C., 2010. Update on CO2 emissions. Nat. Geosci. 3, 811–812. https://doi.org/10.1038/ngeo1022.

Galadima, A., Muraza, O., 2019. Catalytic thermal conversion of CO2 into fuels: perspective and challenges. Renew. Sustain. Energy Rev. 115,. https://doi.org/10.1016/j.rser.2019.109333 109333.

Gallon, H.J., Tu, X., Whitehead, J.C., 2012. Effects of reactor packing materials on H2 production by CO2 reforming of CH4 in a dielectric barrier discharge. Plasma Process. Polym. 9, 90–97. https://doi.org/10.1002/ppap.201100130.

Garcia-Cosio, G., Martinez, H., Calixto-Rodriguez, M., Gomez, A., 2011. DC discharge experiment in an Ar/N2/CO2 ternary mixture: a laboratory simulation of the Martian ionosphere's plasma environment. J. Quant. Spectrosc. Radiat. Transf. 112, 2787–2793. https://doi.org/10.1016/j.jqsrt.2011.09.008.

George, A., Shen, B., Craven, M., Wang, Y., Kang, D., Wu, C., Tu, X., 2021. A review of non-thermal plasma technology: a novel solution for CO2 conversion and utilization. Renew. Sustain. Energy Rev. 135,. https://doi.org/10.1016/j.rser.2020.109702 109702.

Ghiat, I., Al-Ansari, T., 2021. A review of carbon capture and utilisation as a CO2 abatement opportunity within the EWF nexus. J. CO2 Util. 45, 101432.

Gibbins, J., Chalmers, H., 2008. Carbon capture and storage. Energy Policy 36, 4317–4322. https://doi.org/10.1016/j.enpol.2008.09.058.

Hagelaar, G.J.M., Pitchford, L.C., 2005. Solving the Boltzmann equation to obtain electron transport coefficients and rate coefficients for fluid models. Plasma Sources Sci. Technol. 14, 722–733. https://doi.org/10.1088/0963-0252/14/4/011.

He, Y., Wang, Y., Zhang, L., Teng, B., Fan, M., 2015. High-efficiency conversion of CO2 to fuel over ZnO/g-C3N4 photocatalyst. Appl. Catal. B Environ. 168–169, 1–8. https://doi.org/10.1016/j.apcatb.2014.12.017.

Hou, X., Amais, R.S., Jones, B.T., Donati, G.L., 2016. Inductively coupled plasma optical emission spectrometry. Encycl. Anal. Chem., 25

Huang, Q., Zhang, D., Wang, D., Liu, K., Kleyn, A.W., 2017. Carbon dioxide dissociation in non-thermal radiofrequency and microwave plasma, J. Phys. Appl. Phys. 50, 294001. doi: 10.1088/1361-6463/aa754e.

Indarto, A., Yang, D.R., Choi, J.-W., Lee, H., Song, H.K., 2007. Gliding arc plasma processing of CO2 conversion. J. Hazard. Mater. 146, 309–315. https://doi.org/10.1016/j.jhazmat.2006.12.023.

Khan, M.I., Rehman, N.U., Khan, S., Ullah, N., Masood, A., Ullah, A., 2019. Spectroscopic study of CO2 and CO2–N2 mixture plasma using dielectric barrier discharge, AIP Adv. 9, 085015. doi: 10.1063/1.5096399.

Kozák, T., Bogaerts, A., 2014. Splitting of CO2by vibrational excitation in non-equilibrium plasmas: a reaction kinetics model. Plasma Sources Sci. Technol. 23,. https://doi.org/10.1088/0963-0252/23/4/045004 045004.

Lashof, D.A., Ahuja, D.R., 1990. Relative contributions of greenhouse gas emissions to global warming. Nature 344, 529–531. https://doi.org/10.1038/344529a0.

Li, X., Zhao, N., Fang, T., Liu, Z., Li, L., Dong, L., 2008. Characteristics of an atmospheric pressure argon glow discharge in a coaxial electrode geometry. Plasma Sources Sci. Technol. 17 (1), 015017.

Lu, N., Sun, D., Zhang, C., Jiang, N., Shang, K., Bao, X., Li, J., Wu, Y., 2018. CO2 conversion in non-thermal plasma and plasma/g-C3N4catalyst hybrid processes. J. Phys. Appl. Phys. 51, 094001. doi: 10.1088/1361-6463/aaa919.

Mei, D., Zhu, X., He, Y.-L., Yan, J.D., Tu, X., 2014. Plasma-assisted conversion of CO2 in a dielectric barrier discharge reactor: understanding the effect of packing materials. Plasma Sources Sci. Technol. 24, 015011.

Mei, D., Tu, X., 2017. Conversion of CO2 in a cylindrical dielectric barrier discharge reactor: Effects of plasma processing parameters and reactor design. J. CO2 Util. 19, 68–78. https://doi.org/10.1016/j.jcou.2017.02.015.

Mei, D., He, Y.-L., Liu, S., Yan, J., Tu, X., 2016. Optimization of CO2 conversion in a cylindrical dielectric barrier discharge reactor using design of experiments. Plasma Process. Polym. 13 (5), 544–556.

Mei, D., Zhu, X., Wu, C., Ashford, B., Williams, P.T., Tu, X., 2016. Plasma-photocatalytic conversion of CO2 at low temperatures: understanding the synergistic effect of plasma-catalysis. Appl. Catal. B Environ. 182, 525–532. https://doi.org/10.1016/j.apcatb.2015.09.052.

Michielsen, I., Uytdenhouwen, Y., Pype, J., Michielsen, B., Mertens, J., Reniers, F., Meynen, V., Bogaerts, A., 2017. CO2 dissociation in a packed bed DBD reactor: first steps towards a better understanding of plasma catalysis. Chem. Eng. J. 326, 477–488. https://doi.org/10.1016/j.cej.2017.05.177.

Nguyen, H.P., Park, M.J., Kim, S.B., Kim, H.J., Baik, L.J., Jo, Y.M., 2018. Effective dielectric barrier discharge reactor operation for decomposition of volatile organic compounds. J. Clean. Prod. 198, 1232–1238.

Pancheshnyi, S., Biagi, S., Bordage, M.C., Hagelaar, G.J.M., Morgan, W.L., Phelps, A.V., Pitchford, L.C., 2012. The LXCat project: electron scattering cross sections and swarm parameters for low temperature plasma modeling. Chem. Phys. 398, 148–153.

Parastaev, A., Hoeben, W.F.L.M., van Heesch, B.E.J.M., Kosinov, N., Hensen, E.J.M., 2018. Temperature-programmed plasma surface reaction: an approach to determine plasma-catalytic performance. Appl. Catal. B Environ. 239, 168–177. https://doi.org/10.1016/j.apcatb.2018.08.011.

Petrović, D., Martens, T., van Dijk, J., Brok, W.J.M., Bogaerts, A., 2009. Fluid modelling of an atmospheric pressure dielectric barrier discharge in cylindrical geometry. J. Phys. Appl. Phys. 42, 205206. doi: 10.1088/0022-3727/42/20/205206.

Pitchford, L.C., Alves, L.L., Bartschat, K., Biagi, S.F., Bordage, M.-C., Bray, I., Brion, C.E., Brunger, M.J., Campbell, L., Chachereau, A., 2017. Lxcat: an open-access, web-based platform for data needed for modeling low temperature plasmas. Plasma Process. Polym. 14, 1600098.

Qiao, J., Liu, Y., Hong, F., Zhang, J., 2014. A review of catalysts for the electroreduction of carbon dioxide to produce low-carbon fuels. Chem. Soc. Rev. 43, 631–675. https://doi.org/10.1039/c3cs60323g.

Quigley, K.M., Althoff, A.G., Donati, G.L., 2016. Inductively coupled plasma optical emission spectrometry as a reference method for silicon estimation by near infrared spectroscopy and potential application to global-scale studies of plant chemistry. Microchem. J. 129, 231–235. https://doi.org/10.1016/j.microc.2016.06.028.

Ray, D., Chawdhury, P., Subrahmanyam, Ch., 2020. 1. A facile method to decompose CO2 using a g-C3N4-assisted DBD plasma reactor. Environ. Res. 183,. https://doi.org/10.1016/j.envres.2020.109286 109286.

Ray, D., Subrahmanyam, C., 2016. 11. CO2 decomposition in a packed DBD plasma reactor: influence of packing materials. RSC Adv. 6, 39492–39499. doi: 10.1039/C5RA27085E.

Ray, D., Chawdhury, P., Bhargavi, K.V.S.S., Thatikonda, S., Lingaiah, N., Subrahmanyam, Ch., 2021. 2.Ni and Cu oxide supported γ-Al2O3 packed DBD plasma reactor for CO2 activation, J. CO2 Util. 44, 101400. doi: 10.1016/j.jcou.2020.101400.

Retallack, G.J., Conde, G.D., 2020. Deep time perspective on rising atmospheric CO2. Glob. Planet. Change. 189,. https://doi.org/10.1016/j.gloplacha.2020.103177 103177.

Skjånes, K., Lindblad, P., Muller, J., 2007. BioCO2–A multidisciplinary, biological approach using solar energy to capture CO2 while producing H2 and high value products. Biomol. Eng. 24 (4), 405–413.

Wang, Y., Chen, Y., Harding, J., He, H., Bogaerts, A., Tu, X., 2022. Catalyst-free single-step plasma reforming of CH4 and CO2 to higher value oxygenates under ambient conditions. Chem. Eng. J. 450,. https://doi.org/10.1016/j.cej.2022.137860 137860.

Wang, T., Liu, H., Xiong, X., Feng, X., 2017. Conversion of carbon dioxide to carbon monoxide by pulse dielectric barrier discharge plasma. IOP Conf. Ser. Earth Environ. Sci. 52,. https://doi.org/10.1088/1742-6596/52/1/012100 012100.

Wang, R., Yang, Y., Chen, S., Jiang, H., Martin, P., 2021. Power calculation of pulse power-driven DBD plasma. IEEE Trans. Plasma Sci. 49, 2210–2216. https://doi.org/10.1109/TPS.2021.3084601.

Wang, L., Yi, Y., Guo, H., Tu, X., 2018. Atmospheric pressure and room temperature synthesis of methanol through plasma-catalytic hydrogenation of CO_2. ACS Catal. 8, 90–100. https://doi.org/10.1021/acscatal.7b02733.

Xu, S., Whitehead, J.C., Martin, P.A., 2017. CO2 conversion in a non-thermal, barium titanate packed bed plasma reactor: the effect of dilution by Ar and N2. Chem. Eng. J. 327, 764–773. https://doi.org/10.1016/j.cej.2017.06.090.

Yap, D., Tatibouët, J.-M., Batiot-Dupeyrat, C., 2015. Carbon dioxide dissociation to carbon monoxide by non-thermal plasma. J. CO2 Util. 12, 54–61. https://doi.org/10.1016/j.jcou.2015.07.002.

Zeng, S., Kar, P., Thakur, U.K., Shankar, K., 2018. A review on photocatalytic CO2 reduction using perovskite oxide nanomaterials. Nanotechnology 29, 052001. doi: 10.1088/1361-6528/aa9fb1.

Zhang, K., Zhang, G., Liu, X., Phan, A.N., Luo, K., 2017. A study on CO2 decomposition to CO and O2 by the combination of catalysis and dielectric-barrier discharges at low temperatures and ambient pressure. Ind. Eng. Chem. Res. 56, 3204–3216. https://doi.org/10.1021/acs.iecr.6b04570.

Zhu, X., Gao, X., Zheng, C., Wang, Z., Ni, M., Tu, X., 2014. Plasma-catalytic removal of a low concentration of acetone in humid conditions. RSC Adv. 4, 37796–37805. https://doi.org/10.1039/C4RA05985A.